Titanium dioxide induces apoptosis under UVA irradiation via the generation of lysosomal membrane permeabilization-dependent reactive oxygen species in HaCaT cells

In Young Kim
Korea Research Institute of Standards and Science
Tae Geol Lee
Korea Research Institute of Standards and Science
Vytas Reipa
National Institute of Standards and Technology
Min Beom Heo (mbheo@kriss.re.kr)
Korea Research Institute of Standards and Science

Research

Keywords: titanium dioxide nanoparticles (TiO2 NPs), ultraviolet A (UVA), photocytotoxicity, lysosomal membrane permeabilization (LMP), reactive oxygen species (ROS)

Posted Date: March 18th, 2021

DOI: https://doi.org/10.21203/rs.3.rs-315515/v1

Abstract

Background Titanium dioxide nanoparticles (TiO_2 NPs) are important nanomaterials with wide commercial applications. While the small size of TiO_2 NPs is useful in various applications, their biosafety should be evaluated further. In this study, we investigated the cytotoxicity of TiO_2 NPs in the presence and absence of UVA irradiation in human keratinocyte HaCaT cells.

Results TiO_2 NPs did not significantly affect cell viability in the absence of UVA irradiation. However, UVA-irradiated TiO_2 NPs induced caspase-dependent apoptosis. Exposure of HaCaT cells to TiO_2 NPs and UVA resulted in reactive oxygen species (ROS) generation, and lysosomal membrane permeabilization (LMP); both effects were absent without UVA irradiation. An analysis of the relationship between LMP and ROS, using CA-074 as a cathepsin inhibitor or NAC as an antioxidant, showed that LMP stimulates ROS generation under these conditions.

Conclusion These results imply that LMP-dependent oxidative stress plays a critical role in the UVA phototoxicity of TiO_2 NPs in HaCaT cells.

Background

The potential toxicity of nanomaterials (NMs) to humans and the environment has been recognized in modern nanotechnology [1]. This is because their physicochemical properties are highly dependent on the small particle size resulting in a high surface-to-volume ratio and enhanced transport across biological barriers [2]. Consequently, some materials, while they are benign in the bulk form, become toxic when prepared in nano sizes [3].

Titanium dioxide nanoparticles (TiO_2 NPs) are the highest volume-NM employed in water purification, paint, food additives, and personal care products, including sunscreens. There is a high probability that these nanoparticles (NPs) will come in contact with human skin and mucous membranes during their life cycle, with the subsequent entry into the body [4]. Numerous studies have confirmed that the overall cytotoxicity of TiO_2 NPs is rather low compared with many widely produced NMs [5–7], and they are “generally regarded as safe” by regulatory agencies [8]. On the contrary, *in vitro* studies with mammalian cells have shown that TiO_2 NPs induced oxidative stress and apoptosis [9–12], suggesting that the safety profile of TiO_2 NPs is still unclear.

A key determinant of NPs toxicity is their ability to translocate cellular membranes and their subcellular localization. NPs typically accumulate in the lysosomes [13] via processes such as autophagy and endocytosis. Autophagy, a main catabolic pathway in mammalian cells, is involved in the elimination of foreign substances and cell degradation products by encapsulating them with a double membrane thus forming the autophagosome and subsequent fusion with a lysosome. Following their fusion, substances in autophagosomes are digested by lysosomal hydrolytic enzymes. Impairment of this process can lead to a variety of human diseases, and at a molecular level, it is linked to the damage of specific autophagy

system components such as lysosomes. The uptake and accumulation of positively charged polystyrene nanoparticles have been found to cause progressive lysosomal alterations, from the early mild lysosomal membrane permeabilization (LMP), followed by lysosomal expansion and extensive LMP [13] at prolonged exposures. Substantial lysosomal damage leads to cathepsin release, thereby inducing cell apoptosis and necrosis [13–15]. A 24 h exposure to TiO_2 NPs of various sizes has been found to induce the upregulation of autophagic flux, lysosomal dysfunction, and membrane permeabilization, whereas a 72 h exposure promoted the blockage in autophagic flux [16–17].

Interest in TiO_2 NPs is mostly related to their photocatalytic activity which is a major contributor to the toxicological effects if TIO_2 NPs when they interact with biomolecules [18–19]. Phototoxicity is triggered by adverse chemical reactions supported by photocatalytically active material under illumination. The principal cause of cell death mediated by photoactivated TiO_2 NPs is the oxidative damage of proteins, nucleic acids, and lipids caused by excessive ROS generation when TiO_2 NP absorb UV light and the excited charge carriers react with oxygen and/or water [20]. Therefore, the safety of TiO_2 NPs is highly dependent on lighting conditions during their human and environmental exposure [21].

Due to the lack of clarity regarding the effects of the photocatalytic activity of TiO_2 NP on the human body, some regulators have restricted their use in cosmetic applications, including sunscreens [22]. Photocatalytic activity is a well-established physicochemical property of TiO_2 NPs and is directly related to cellular toxicity under ultraviolet (UV) irradiation [23–24]. These properties also serve as a basis for the development of photodynamic therapies as TiO_2 NPs under UVA irradiation ($310\ nm < \lambda < 390\ nm$) induce cell death in colon carcinoma, melanoma, cervix adenocarcinoma, fibroblasts, and keratinocytes [25–30].

Given the increased interest in the nanomedical application of photoexcited TiO_2 NPs and concerns about their safety in personal care products, the mechanistic aspects of cell impairment have lately become a focus of experimental studies [31–32]. Besides the photoproduction of ROS and ensuing oxidative stress as the underlying factor for the adverse biological reactions, other attributes such as NP subcellular localization alter the phototoxic effects of TiO_2 NPs. Photo-induced damage to the endoplasmic reticulum often leads to cell death by autophagy [33]. A significant increase in the number of autophagic vesicles along with the degradation of the endoplasmic reticulum, but no inflammation, was observed by Yu et al. [34] in TiO_2-exposed human bronchial epithelial cells. Moreover, TiO_2 NP-generated ROS can also promote the uncoupling of the mitochondrial respiratory chains resulting in excess intracellular ROS production from the superoxide anion [35]. Other studies show that UV irradiation aggravates LMP, which leads to the intrinsic apoptosis of melanocytes [36–37] as well as cell necroptosis by hindering autophagosome-lysosome fusion [38]. These findings suggest that the role of photoexcitation in autophagy and lysosomal damage is not well established [39]. In this study, we focused on the mutual effects of TiO_2 NP uptake in HaCaT cells and UVA sensitization on lysosomal membrane integrity. We found evidence that major lysosomal destabilization occurs when accumulated TiO_2 NPs are photoexcited by UVA. Consequently, the loss of lysosomal membrane integrity is essential for TiO_2 NPs and UVA-induced ROS surge. Taken together, our data strongly suggest that caspase-

dependent apoptosis is a key mechanism of HaCaT cell death induced by their exposure to photoexcited TiO_2 NPs.

Results

Characterization of the TiO_2 NP suspension employed for cellular exposure

DLS was performed to determine the particle size distribution in TiO_2 NP suspension (Fig. 2). After dispersion in media, the average size of TiO_2 NPs was 221.6 ± 0.9 nm (intensity) with a polydispersity index of 0.246 (Fig. 2a). In addition, the stability of the TiO_2 NP suspension during the test duration was tested. The particle size distribution profile was constant for 2 days (Fig. 2b), indicative of the stability of the TiO_2 NP suspension.

UVA irradiation induces toxicity in HaCaT cells treated with TiO_2 NPs

We investigated whether the viability of human keratinocytes, HaCaT cells, is affected by a combination of TiO_2 NPs and UVA irradiation. Cell viability measurement demonstrated that HaCaT cells were resistant to both TiO_2 exposure (200 μg/mL) and UVA irradiation treatment separately (Fig. 3a). However, a combination of TiO_2 NPs and UVA irradiation markedly reduced the viability of HaCaT cells (Fig. 3a). To quantify TiO_2 NP phototoxicity, we estimated the NP concentrations, which inhibit 50% of cell growth (IC_{50} value) with and without UVA irradiation. The IC_{50} of the samples was reduced 10-fold with UVA irradiation compared to non-irradiated samples (Fig. 3a). To confirm cellular damage, we performed the LDH assay. TiO_2 NPs alone at low concentrations < 100 μg/mL did not induce a noticeable LDH release. However, the LDH activity was boosted in cells that were subjected to combined treatment than in those treated with TiO_2 NPs alone (Fig. 3b). Collectively, these results confirm that TiO_2 NPs cause pronounced cytotoxicity under UVA irradiation.

UVA irradiation facilitates the apoptosis of HaCaT cells treated with TiO_2 NPs

Next, we examined the morphological changes in cells that occurred during combined TiO_2 NP and UVA treatment. The cells treated with TiO_2 NPs or UVA irradiation separately remained attached to the substrate, and largely retained their size. In contrast, the cells treated with both TiO_2 NPs and UVA irradiation detached from the plate surface became smaller and spherical (Fig. 4a). Given that cell shrinkage, or cell volume loss, is often an indication of apoptosis [40], we wanted to verify whether the cell death induced by combined treatment with TiO_2 NPs and UVA was apoptotic. We examined the changes in DNA content following treatment with TiO_2 NPs and UVA irradiation (Fig. 4b). Only 11.8% of HaCaT cells treated with TiO_2 NPs alone for 24 h were in the sub-G1 phase, and there was no significant change in the DNA content. However, when both NP and UVA treatments were performed, a 31.4% increase in the sub-G1 population was recorded. This result provides further evidence that a combination of TiO_2 and UVA leads to HaCaT cell death via the apoptotic pathway.

We also examined whether the combination of TiO_2 NP and UVA-induced cell death was mediated by caspase activation. Again, we found no evidence that caspase substrate, poly (ADP-ribose) polymerase (PARP) was processed following the treatment of HaCaT cells with either TiO_2 NPs or UVA (Fig. 4c). However, when both TiO_2 NPs and UVA were applied, PARP was progressively processed (Fig. 4c). To ascertain whether caspases are important in apoptosis induced by the combination of TiO_2 NPs and UVA, we investigated the effect of a pan-caspase inhibitor z-VAD-fmk in cell viability. The treatment of HaCaT cells with z-VAD-fmk dose-dependently blocked co-treatment-induced cell death (Fig. 4d). Taken together, these results show that TiO_2 NPs under UVA irradiation induces caspase-dependent apoptosis of HaCaT cells.

TiO_2 NPs accumulate in lysosomes

To observe the cellular uptake of TiO_2 NPs and structural changes in the cellular organelles in TiO_2 NP and UVA-treated cells, we examined the electron microscopy images acquired (Fig. 5). First, we confirmed the cellular uptake of TiO_2 NPs. TiO_2 NPs were not detected in untreated or just UVA-irradiated cells (Fig. 5a, 5c). Both after treatment with TiO_2 NPs alone and in combination with UVA, TiO_2 NPs were observed in an aggregate form in the phagosome-like structures (black arrowhead), but not in the nuclei (white arrow) or mitochondria (black arrow) (Fig. 5b, 5d). Next, we observed alterations in the cellular organelle structures. The organelles did not dramatically change except when treated with both TiO_2 NPs and UVA (Fig. 5a–5c). Remarkably, the mitochondrial structure remained almost unaltered in all the imaged samples (Fig. 5, black arrow). Moreover, we found that the combination of TiO_2 NPs and UVA increased the number of phagosomal and lysosomal structures containing TiO_2 NPs (Fig. 5d, black arrowhead). These membranes were noticeably ruptured (Fig. 5d, white arrowhead).

Combination of TiO_2 NPs and UVA induces lysosomal membrane permeabilization

As our results suggested that lysosomal membranes were altered by the combination of TiO_2 NPs and UVA (e.g., ruptured membranes in Fig. 5), we tested the lysosomal integrity of HaCaT cells by staining them with AO. While red fluorescence was strong, green fluorescence was weak in untreated cells. However, the cells treated with TiO_2 NPs and UVA mostly showed diminished red fluorescence and increased green fluorescence (Fig. 6a), indicating that the lysosomes were severely damaged. Next, we quantified the lysosomal integrity using a microplate reader. The integrity of the lysosomes in cells treated with the combination of TiO_2 NPs and UVA decreased to 89.04% ± 3.98% and 86.02% ± 4.01% following incubation with 100 μg/mL and 200 μg/mL TiO_2 NPs, respectively, relative to lysosomes in pristine cells (100%) (Fig. 6b). These results suggest that lysosomal membranes are subjected to damage during HaCaT cell death triggered by combined treatment with TiO_2 NPs and UVA.

Combination of TiO_2 NPs and UVA generates reactive oxygen species

The oxidative damage of cellular molecules caused by excessive ROS production is known as a major factor driving the phototoxicity of TiO_2 NPs [25–29]. In this study, we assayed intracellular ROS production using CM-H_2DCF-DA dye. Independent treatment with TiO_2-NPs and UVA generated rather low

levels of intracellular ROS in a concentration-dependent manner (Fig. 6c) while the combination of TiO_2 NPs and UVA significantly increased intracellular ROS. This was particularly noticeable in the cells treated with 200 μg/mL TiO_2 NPs, wherein, the intracellular ROS level increased by approximately 2.3-fold following treatment with UVA irradiation compared with the non-irradiated sample (Fig. 6c). Fluorescence microscopy images confirmed that TiO_2 NPs and UVA noticeably increased the ROS levels when combined (Fig. 6d). These results confirm that intracellular ROS are produced during HaCaT cell death caused by the combination of TiO_2 NPs and UVA

The relation between LMP, ROS generation, and cell death in HaCaT cells treated with TiO_2 NPs and UVA

We examined the link between the lysosomal membrane damage, ROS generation, and cell death induced by the combination of TiO_2 NPs and UVA. First, we assessed the involvement of lysosomal membrane damage and ROS generation in cell death using CA-074, a cathepsin B inhibitor, and NAC, a well-known antioxidant. When the medium was replaced after TiO_2 NP treatment and UVA irradiation, each inhibitor was added to the media, and the cells were incubated for 24 h. The treatment of HaCaT cells with CA-074 and NAC effectively inhibited the cell death caused by the combination of TiO_2 NPs and UVA (Fig. 7a). This result implies that both lysosomal membrane damage and ROS generation are critical contributors to cell death under these conditions.

Next, we investigated the relationship between lysosomal membrane damage and ROS generation. ROS are known to induce LMP, especially when highly reactive hydroxyl radicals are produced in the lysosomes [41–43]. Therefore, we wanted to determine whether the loss of lysosomal membrane integrity occurs when ROS are produced in response to the combined TiO_2 NPs and UVA treatment. Surprisingly, neither CA-074 nor NAC affected lysosomal membrane integrity in cells treated with TiO_2 NPs and UVA (Fig. 7b). This result indicates that ROS did not decrease lysosomal membrane integrity. Further, as LMP may increase the generation of intracellular ROS via the release of free iron into the cytosol [44–46], we evaluated whether ROS can be generated due to LMP. Interestingly, both CA-074 and NAC attenuated ROS generation in response to the combined treatment with TiO_2 NPs and UVA (Fig. 7c). This result suggests that the loss of lysosomal membrane integrity is vital for TiO_2 NP and UVA-induced ROS generation. Taken together, these results show that the combination of TiO_2 NPs and UVA induces cell death via LMP-dependent ROS generation in HaCaT cells.

Discussion

TiO_2 NPs are among the most widely used nanomaterials in paints, plastics, cosmetics, and personal care products; they are also used as food additives and drug delivery agents [47–48]. They are widely used owing to their good biocompatibility, high chemical stability, photocatalytic properties, and pronounced sensitivity to heat and magnetism [49–51]. In particular, TiO_2 NPs are potential candidates for degrading organic pollutants [52] and inactivating microorganisms owing to their photocatalytic activity [47, 53]. However, these photocatalytic properties were reported to trigger oxidative damage,

cellular structure destruction, key protein inactivation, and DNA damage, leading to cell apoptosis or necrosis [54–57]. To support their safe and efficient use, it is essential to identify mechanisms underlying the photocatalytic activity and phototoxicity of TiO_2 NPs. In this study, we evaluated the phototoxicity of TiO_2 NPs on human skin keratinocytes subjected to UVA irradiation and investigated the mechanistic aspects of the resulting cell death.

As shown in Fig. 3, TiO_2 NPs exerted UVA-induced and dose-dependent toxicity in HaCaT cells. As cell viability decreases after TiO_2 NP and UVA treatment, we explored the mode of death in these cells. The photocatalytic activity of TiO_2 NPs can induce apoptosis and necrosis through various mechanisms [54–55, 57–59]. Apoptosis is a form of programmed cell death characterized by caspase activation, cell contraction, apoptotic body formation, exposure outside the cell membrane, chromatic condensation, and DNA fragmentation [60–62]. Our data show that the DNA sub-G1 population increases following combined treatment with TiO_2 NPs and UVA (Fig. 4b). In addition, PARP, a substrate of caspase-3, is cleaved and z-VAD-fmk, a pan-caspase inhibitor, increases the viability in HaCaT cells co-treated with TiO_2 NPs and UVA (Fig. 4c, 4d). These results suggest that the TiO_2 NPs and UVA-induced cell death is caused by caspase-dependent apoptosis.

We detected TiO_2 NPs inside HaCaT cells using transmission electron microscopy, thereby demonstrating that the phototoxicity observed in this study is induced by the intracellular accumulation of TiO_2 NPs. Consistent with the results of Tucci et al. [63], TiO_2 NPs accumulated in the phagosomal and lysosomal structures of the cells, but not in the nuclei or mitochondria (Fig. 5b, 5d). Remarkably, we observed lysosomal membrane rupture in HaCaT cells treated with TiO_2 NPs and UVA (Fig. 5d). The maintenance of lysosomal membrane integrity is vital for cell viability because ruptured lysosomal membranes induce the leakage of various digestive enzymes into the cytosol, resulting in membrane trafficking defects, abnormal energy metabolism, and cell death [64]. Recently, lysosomal damage has been suggested as a key mechanistic element of nanoparticle toxicity [65–67] because most endocytosed nanoparticles were found to accumulate in lysosomal compartments. In our study, we evaluated the lysosomal membrane integrity by AO staining and determined that combined treatment with TiO_2 NPs and UVA damaged the lysosomal membranes in HaCaT cells (Fig. 6a, 6b). In addition, CA-074, a cathepsin B inhibitor that protects against lysosomal rupture [68], prevented cell death induced by the combination of TiO_2 NPs and UVA (Fig. 7A). These results demonstrate that LMP is imperative for TiO_2 NP and UVA-induced cell death.

As ROS-mediated LMP is the prevailing mechanism [69], we examined the link between LMP and ROS generation when HaCaT cells are exposed to TiO_2 NPs and UVA. First, we found that TiO_2 NPs subjected to UVA irradiation upregulated ROS generation inside the HaCaT cells (Fig. 6c-6d). In addition, the inhibition of ROS increased cell viability (Fig. 7a), confirming the critical regulatory role of ROS in the progression of HaCaT cell apoptosis. Next, we tested lysosomal membrane integrity and ROS production in cells treated with a cathepsin B inhibitor CA-074 and antioxidant NAC. Interestingly, while CA-074 prevented ROS generation, NAC did not prevent the loss of lysosomal membrane integrity (Fig. 7b, 7c). Although several factors and chemicals have been reported to induce LMP and the associated cell death

[70–72], it is not clear whether lysosomal leakage leads to oxidative stress during apoptotic cell death driven by the lysosomal pathway. Our study, for the first time, proves that lysosomal destabilization by TiO_2 NPs and UVA induces cellular ROS generation and oxidative stress.

Conclusions

In this study, we confirmed TiO_2 NP phototoxicity to human keratinocytes due to their photocatalytic activity when exposed to UVA light. TiO_2 NPs in the dark appeared to be non-toxic, whereas internalized TiO_2 NPs caused apoptosis via LMP-mediated ROS generation in HaCaT cells under UVA irradiation. The internalization of TiO_2 NPs is linked to lysosomal destabilization under UVA irradiation, leading to intracellular ROS generation and apoptotic cell death. Our results point toward a novel mechanistic pathway for the phototoxicity of UVA-exposed TiO_2 NPs *in vitro*.

Methods

Chemicals

z-VAD-fmk was purchased from R&D system (Minneapolis, MN, USA). 5-(and-6)-chloromethyl-2',7'-dichlorodihydrofluorescein diacetate, acetyl ester (CM-H_2DCF-DA) was purchased from Thermo Fisher Scientific (Waltham, MA, USA). Propidium iodide, N-acetyl-L-cysteine (NAC), (L-3-trans-(propylcarbamyl)oxirane-2-carbonyl)-L-isoleucyl-L-proline (CA-074), and acridine orange (AO) were purchased from Sigma-Aldrich (St. Louis, MO, USA).

Cell culture

Human keratinocyte HaCaT cells (Cell Line Services, Eppelheim, Germany) were maintained in Dulbecco's modified Eagle medium containing 10% fetal bovine serum and 1% penicillin–streptomycin (all obtained from GIBCO-BRL (Grand Island, NY, USA). The cells were incubated under 5% CO_2 at 37°C.

Preparation and characterization of TiO_2 NP suspension

TiO_2 NPs (AEROXIDE® TiO_2 P25) were obtained from Evonik Industries AG (Essen, Germany). They were dispersed in a complete medium according to the National Institute of Standards and Technology special publication 1200–4 [73]. Particle size distribution of TiO_2 NPs was obtained by dynamic light scattering (DLS; ZEN5600, Malvern Panalytical, Worcestershire, England).

Treatment with TiO_2 NPs and UV

A graphic summary of the experimental procedure is shown in Fig. 1. HaCaT cells were inoculated in two 96-well plates and then incubated for 24 h. On the subsequent day, the surface adhered cells were exposed to TiO_2 NPs for 24 h at 25–200 μg/mL. The treated cells were washed twice with warm PBS to separate extracellular TiO_2 NPs. Subsequently, PBS was replaced with Hanks' balanced salt solution (HBSS) (GIBCO-BRL) to avoid UVA light attenuation by light-absorbing components during the irradiation. While one plate was directly irradiated with UVA for 20 min (light dose P = 5 J/cm^2, exposure group), the

other plate was protected from UVA exposure using foil (dark group). Following the post-irradiation stabilization for 20 min, HBSS was replaced with a complete medium, and the cells were incubated for 24 h.

Cell viability assay

The cells were seeded in 96-well plates and treated as described above. The CellTiter-Glo Luminescent Cell Viability kit (Promega, Madison, WI, USA) was employed to assess cell viability, according to the manufacturer's instructions. The IC_{50} value, the concentration at which cell growth is inhibited by 50% compared with the untreated control, was estimated using GraphPad Prism software 7.0 (GraphPad Software Inc., San Diego, CA, USA).

Measurement of lactate dehydrogenase release

A lactate dehydrogenase (LDH) detection kit (CytoTox96® Non-Radioactive Cytotoxicity Assay, Promega) was used to evaluate the integrity of the cell membrane. The release of LDH into the culture medium indicates irreversible cell death due to cell membrane damage [74–75]. After treating the cells as mentioned above, 50 µL of the supernatant was collected and tested according to the manufacturer's instructions.

Cell cycle analysis

DNA fragmentation is a hallmark of apoptosis [40] and, therefore, apoptotic cells eventually develop a deficit in DNA content. In DNA content histograms, apoptotic cells often form characteristic "sub-G1" or "hypodiploid" peaks [76–78]. After treatment, HaCaT cells were harvested and fixed in 70% (v/v) ethanol. To evaluate DNA content, the cells were stained with propidium iodide and analyzed using a FACSVerse flow cytometer (BD Biosciences, San Jose, CA, USA). The data were analyzed using FlowJo (version X, BD Biosciences).

Cell lysates and western blotting

HaCaT cells were seeded in 60-mm dishes and treated as mentioned above. The treated cells were scrapped and harvested using PBS. After discarding the supernatant, the cell pellets were suspended in 2× Laemmli sample buffer with 5% β-mercaptoethanol (Bio-Rad, Hercules, CA, USA), and boiled for 7 min. The lysates were separated by 4–15% SDS-PAGE and transferred onto an Immobilon membrane (Millipore, Burlington, MA, USA). In this study, the following primary antibodies were used: PARP1 (1:1000, ab32071, Abcam, Cambridge, UK) and β-actin (1:5000, #3700, Cell Signaling Technology, Beverly, MA, USA). The secondary antibodies used were horseradish peroxidase (HRP)-conjugated goat anti-rabbit immunoglobulin G (IgG) and goat anti-mouse IgG (Invitrogen, Waltham, MA, USA). Bands were developed using WesternBright ECL HRP substrate (Advansta, CA, USA). Quantification of the immunoblots was performed using Image J (NIH).

Lysosomal integrity assay

Because AO is a lysosomotropic dye that exhibits a red fluorescence under acidic conditions and green fluorescence under non-acidic conditions, lysosomal acidification can be predicted through the green/red

fluorescence ratio in live cells [79]. We followed the method described by Sun and Gan [80]. For fluorescence microscopy, HaCaT cells were seeded in 12-well plates and treated as mentioned above. After washing with PBS, the cells were stained with 5 µg/mL AO in DMEM for 15 min in the dark at 37°C. The cells were washed with PBS again and further visualized using a fluorescence microscope (Leica Microsystems, Wetzlar, Germany). To quantitate fluorescence using a microplate reader, the cells were seeded in 96-well plates and allowed to sufficiently attach to the plate for 24 h. The cells were stained with 5 µg/mL AO for 15 min. After PBS washing, the cells were subsequently treated with TiO_2 NPs and UVA irradiation. The treated cells were incubated for 8 h, and then washed with HBSS. The fluorescence was measured at an excitation wavelength of 485 nm and two emission wavelengths of 530 (green AO) and 620 nm (red AO). Normal lysosomal integrity = total red fluorescence intensity of normal lysosomes / total green fluorescence intensity of normal lysosomes. Lysosomal integrity = total red fluorescence intensity / (total green fluorescence intensity × normal lysosomal integrity).

Measurement of reactive oxygen species

When CM-H_2DCF-DA is oxidized by ROS such as H_2O_2 and free radicals, it can be detected by monitoring the increase in fluorescence [81]. The treated cells were loaded with 10 µM CM-H_2DCF-DA for 30 min in the dark at 37°C and washed with HBSS. The cells were measured using a microplate reader (ex = 495 nm/em = 525 nm) and observed by fluorescence microscopy.

Transmission electron microscopy

The cells were pre-fixed in Karnovsky's solution (1% paraformaldehyde, 2% glutaraldehyde, 2 mM calcium chloride, and 0.1 M cacodylate buffer, pH 7.4) for 2 h and washed with cacodylate buffer. Post-fixing was carried out in 1% osmium tetroxide and 1.5% potassium ferrocyanide for 1 h. After dehydration with 50–100% alcohol, the cells were embedded in Poly/Bed 812 resin (Pelco, Redding, CA, USA), polymerized, and observed under an electron microscope (EM 902A; Carl Zeiss, Oberkochen, Germany).

Statistical analysis

All data are presented as mean ± standard error of the mean (SEM) or standard deviation (SD) from at least three separate experiments. GraphPad Prism 7.0 software was used to perform statistical analyses. The normality of data was assessed using Kolmogorov–Smirnov test, and equal variance was assessed using Bartlett's test. For normally distributed data, statistical differences were determined using the analysis of variance, followed by Bonferroni's multiple comparison tests. If the data were not normally distributed, Kruskal–Wallis test was performed followed by Dunn's test.

Declarations

Ethics approval and consent to participate

Not applicable.

Consent for publication

Not applicable.

Availability of data and material

The datasets used and/or analyzed during the current study are available from the corresponding author on reasonable request.

Competing interests

The authors have no relevant financial or non-financial interests to disclose.

Funding

This research was supported by the Nano Material Technology Development Program [grant number 2016M3A7B6908929] of the National Research Foundation (NRF) of Korea funded by the Ministry of Science and ICT (MSIT) and Development of Measurement Standards and Technology for biomaterials and Medical Convergence funded by Korea Research Institute of Standards and Science (KRISS – 2021 – GP2021-0004).

Authors' contributions

All authors contributed to the study conception and design. Material preparation and data collection and analysis were performed by In Young Kim, Tae Geol Lee, and Min Beom Heo. The first draft of the manuscript was written by In Young Kim, Vytas Reipa, and Min Beom Heo. All authors commented on previous versions of the manuscript. All authors read and approved the final manuscript.

Acknowlegements

Not applicable.

Authors' information

[1] Safety Measurement Institute, Korea Research Institute of Standards and Science, Daejeon, Republic of Korea. [2] Materials Measurement Laboratory, Biosystems and Biomaterials Division, National Institute of Standards and Technology, Gaithersburg, USA.

References

1. Ferin J, Oberdorster G, Penney DP, Soderholm SC, Gelein R, Piper HC. Increased pulmonary toxicity of ultrafine particles? I. Particle clearance, translocation, morphology. J Aerosol Sci. 1990;21(3):381–4. https://doi.org/10.1016/0021-8502(90)90064-5.
2. Schulte PA, Leso V, Niang M, Iavicoli I. Current state of knowledge on the health effects of engineered nanomaterials in workers: a systematic review of human studies and epidemiological investigations. Scand J Work Environ Health. 2019;45(3):217–38. https://doi.org/10.5271/sjweh.3800.

3. Yordanov YI, Tzankova VI, Yoncheva K. Nanotoxicology: factors, affecting toxicity. Pharmacia. 2018;65:63–71. https://www.academia.edu/40211413/Nanotoxicology_Factors_affecting_toxicity.
4. Xiong S, Tang Y, Ng HS, Zhao X, Jiang Z, Chen Z, et al. Specific surface area of titanium dioxide (TiO2) particles influences cyto- and photo-toxicity. Toxicology. 2013;304:132–40. https://doi.org/10.1016/j.tox.2012.12.015.
5. Peters K, Unger RE, Kirkpatrick CJ, Gatti AM, Monari E. Effects of nano-scaled particles on endothelial cell function in vitro: studies on viability, proliferation and inflammation. J Mater Sci Mater Med. 2004;15(4):321–5. https://doi.org/10.1023/b:jmsm.0000021095.36878.1b.
6. Yamamoto A, Honma R, Sumita M, Hanawa T. Cytotoxicity evaluation of ceramic particles of different sizes and shapes. J Biomed Mater Res A. 2004;68(2):244–56. https://doi.org/10.1002/jbm.a.20020.
7. Zhang Q, Kusaka Y, Sato K, Nakakuki K, Kohyama N, Donaldson K. Differences in the extent of inflammation caused by intratracheal exposure to three ultrafine metals: role of free radicals. J Toxicol Environ Health A. 1998;53(6):423–38. https://doi.org/10.1080/009841098159169.
8. Pippins R, Samson AJ, Trentacost E. FDA, State, and Local Governments Act to Modernize the regulation of sunscreen products in the United States. https://www.arnoldporter.com/en/perspectives/publications/2019/03/fda-state-and-local-governments-act-to-modernize.
9. Carinci F, Volinia S, Pezzetti F, Francioso F, Tosi L, Piattelli A. Titanium-cell interaction: analysis of gene expression profiling. J Biomed Mater Res B Appl Biomater. 2003;66(1):341–6. https://doi.org/10.1002/jbm.b.10021.
10. Gurr JR, Wang AS, Chen CH, Jan KY. Ultrafine titanium dioxide particles in the absence of photoactivation can induce oxidative damage to human bronchial epithelial cells. Toxicology. 2005;213(1–2):66–73. https://doi.org/10.1016/j.tox.2005.05.007.
11. Long TC, Saleh N, Tilton RD, Lowry GV, Veronesi B. Titanium dioxide (P25) produces reactive oxygen species in immortalized brain microglia (BV2): implications for nanoparticle neurotoxicity. Environ Sci Technol. 2006;40(14):4346–52. https://doi.org/10.1021/es060589n.
12. Rahman Q, Lohani M, Dopp E, Pemsel H, Jonas L, Weiss DG, et al. Evidence that ultrafine titanium dioxide induces micronuclei and apoptosis in Syrian hamster embryo fibroblasts. Environ Health Perspect. 2002;110(8):797–800. https://doi.org/10.1289/ehp.02110797.
13. Wang F, Salvati A, Boya P. Lysosome-dependent cell death and deregulated autophagy induced by amine-modified polystyrene nanoparticles. Open Biol. 2018;8(4):170271. https://doi.org/10.1098/rsob.170271.
14. Kroemer G, Jäättelä M. Lysosomes and autophagy in cell death control. Nat Rev Cancer. 2005;5(11):886–97. https://doi.org/10.1038/nrc1738.
15. Guicciardi ME, Leist M, Gores GJ. Lysosomes in cell death. Oncogene. 2004;23(16):2881–90. https://doi.org/10.1038/sj.onc.1207512.

16. Popp L, Tran V, Patel R, Segatori L. Autophagic response to cellular exposure to titanium dioxide nanoparticles. Acta Biomater. 2018;79:354–63. https://doi.org/10.1016/j.actbio.2018.08.021.
17. Yu Q, Wang H, Peng Q, Li Y, Liu Z, Li M. Different toxicity of anatase and rutile TiO_2 nanoparticles on macrophages: Involvement of difference in affinity to proteins and phospholipids. J Hazard Mater. 2017;335:125–34. https://doi.org/10.1016/j.jhazmat.2017.04.026.
18. Jovanovic B. Review of titanium dioxide nanoparticle phototoxicity: developing a phototoxicity ratio to correct the endpoint values of toxicity tests. Environ Toxicol Chem. 2015;34(5):1070–7. https://doi.org/10.1002/etc.2891.
19. Park H, Yu M, Kang SK, Yang SI, Kim YJ. Comparison of cellular effects of titanium dioxide nanoparticles with different photocatalytic potential in human keratinocyte, HaCaT cells. Mol Cell Toxicol. 2011;7:67–75. https://doi.org/10.1007/s13273-011-0010-4.
20. Dasari TP, Pathakoti K, Hwang HM. Determination of the mechanism of photoinduced toxicity of selected metal oxide nanoparticles (ZnO, CuO, Co3O4 and TiO2) to E. coli bacteria. J Environ Sci. 2013;25(5):882–8. https://doi.org/10.1016/s1001-0742(12)60152-1.
21. Petersen EJ, Reipa V, Watson SS, Stanley DL, Rabb SA, Nelson BC. DNA damaging potential of photoactivated p25 titanium dioxide nanoparticles. Chem Res Toxicol. 2014;27(10):1877–84. https://doi.org/10.1021/tx500340v.
22. OPINION ON Titanium Dioxide (nano form) COLIPA No S75, revision of 22 April 2014. Scientific Committee on Consumer Safety (SCCS), European Commission, 7–9 https://doi.org/10.2875/543025.
23. Agrios AG, Pichat P. State of the art and perspectives on materials and applications of photocatalysis over TiO2. J Appl Electrochem. 2005;35:655–63. https://doi.org/10.1007/s10800-005-1627-6.
24. Herrmann JM. Heterogeneous photocatalysis: Fundamentals and applications to the removal of various types of aqueous pollutants. Catal Today. 1999;53(1):115–29. https://doi.org/10.1016/S0920-5861(99)00107-8.
25. Horie M, Sugino S, Kato H, Tabei Y, Nakamura A, Yoshida Y. Does photocatalytic activity of TiO2 nanoparticles correspond to photo-cytotoxicity? Cellular uptake of TiO2 nanoparticles is important in their photo-cytotoxicity. Toxicol Mech Methods. 2016;26(4):284–94. https://doi.org/10.1080/15376516.2016.1175530.
26. Seo JW, Chung H, Kim MY, Lee J, Choi IH, Cheon J. Development of water-soluble single-crystalline TiO2 nanoparticles for photocatalytic cancer-cell treatment. Small. 2007;3(5):850–3. https://doi.org/10.1002/smll.200600488.
27. Wang C, Cao S, Tie X, Qiu B, Wu A, Zheng Z. Induction of cytotoxicity by photoexcitation of TiO2 can prolong survival in glioma-bearing mice. Mol Biol Rep. 2011;38(1):523–30. https://doi.org/10.1007/s11033-010-0136-9.
28. Xue C, Luo W, Yang XL. A mechanism for nano-titanium dioxide-induced cytotoxicity in HaCaT cells under UVA irradiation. Biosci Biotechnol Biochem. 2015;79(8):1384–90. https://doi.org/10.1080/09168451.2015.1023248.

29. Yin JJ, Liu J, Ehrenshaft M, Roberts JE, Fu PP, Mason RP, et al. Phototoxicity of nano titanium dioxides in HaCaT keratinocytes–generation of reactive oxygen species and cell damage. Toxicol Appl Pharmacol. 2012;263(1):81–8. https://doi.org/10.1016/j.taap.2012.06.001.
30. Zhang AP, Sun YP. Photocatalytic killing effect of TiO2 nanoparticles on Ls-174-t human colon carcinoma cells. World J Gastroenterol. 2004;10(21):3191–3. https://doi.org/10.3748/wjg.v10.i21.3191.
31. Gomes SIL, Roca CP, von der Kammer F, Scott-Fordsmand JJ, Amorim MJB. Mechanisms of (photo)toxicity of TiO2 nanomaterials (NM103, NM104, NM105): using high-throughput gene expression in Enchytaraeus crypticus. Nanoscale. 2018;10(46):21960–70. https://doi.org/10.1039/c8nr03251c.
32. Kang SJ, Lee YJ, Kim BM, Choi YJ, Chung HW. Cytotoxicity and genotoxicity of titanium dioxide nanoparticles in UVA-irradiated normal peripheral blood lymphocytes. Drug Chem Toxicol. 2011;34(3):277–84. https://doi.org/10.3109/01480545.2010.546800.
33. Kessel D, Reiners JJ Jr. Apoptosis and autophagy after mitochondrial or endoplasmic reticulum photodamage. Photochem Photobiol. 2007;83(5):1024–8. https://doi.org/10.1111/j.1751-1097.2007.00088.x.
34. Yu KN, Chang SH, Park SJ, Lim J, Lee J, Yoon TJ, et al. Titanium dioxide nanoparticles induced endoplasmic reticulum stress-mediated autophagic cell death via mitochondria-associated endoplasmic reticulum membrane disruption in normal lung cells. PLoS One. 2015;10(6):e0131208. https://doi.org/10.1371/journal.pone.0131208.
35. Xue C, Li X, Liu G, Liu W. Evaluation of mitochondrial respirator chain on the generation of reactive oxygen species and cytotoxicity in HaCaT cells induced by nanosized titanium dioxide under UVA irradiation. Int J Toxicol. 2016;35(6):644–53. https://doi.org/10.1177/1091581816661853.
36. Bivik CA, Larsson PK, Kågedal KM, Rosdahl IK, Ollinger KM. UVA/B-induced apoptosis in human melanocytes involves translocation of cathepsins and Bcl-2 family members. J Invest Dermatol. 2006;126(5):1119–27. https://doi/org/10.1038/sj.jid.5700124.
37. Bivik C, Rosdahl I, Ollinger K. Hsp70 protects against UVB induced apoptosis by preventing release of cathepsins and cytochrome c in human melanocytes. Carcinogenesis. 2007;28(3):537–44. https://doi.org/10.1093/carcin/bgl152.
38. Mohammadalipour Z, Rahmati M, Khataee A, Moosavi MA. Differential effects of N-TiO2 nanoparticle and its photo-activated form on autophagy and necroptosis in human melanoma A375 cells. J Cell Physiol. 2020;235(11):8246–59. https://doi.org/10.1002/jcp.29479.
39. Stern ST, Adiseshaiah PP, Crist RM. Autophagy and lysosomal dysfunction as emerging mechanisms of nanomaterial toxicity. Part Fibre Toxicol. 2012;9:20. https://doi.org/10.1186/1743-8977-9-20.
40. Kerr JF, Wyllie AH, Currie AR. Apoptosis: a basic biological phenomenon with wide-ranging implications in tissue kinetics. Br J Cancer. 1972;26(4):239–57. https://doi.org/10.1038/bjc.1972.33.
41. Aits S, Jäättelä M. Lysosomal cell death at a glance. J Cell Sci. 2013;126(Pt 9):1905–12. https://doi.org/10.1242/jcs.091181.

42. Česen MH, Pegan K, Spes A, Turk B. Lysosomal pathways to cell death and their therapeutic applications. Exp Cell Res. 2012;318(11):1245–51. https://doi.org/10.1016/j.yexcr.2012.03.005.
43. Serrano-Puebla A, Boya P. Lysosomal membrane permeabilization in cell death: new evidence and implications for health and disease. Ann N Y Acad Sci. 2016;1371(1):30–44. https://doi.org/10.1111/nyas.12966.
44. Kon K, Kim JS, Jaeschke H, Lemasters JJ. Mitochondrial permeability transition in acetaminophen-induced necrosis and apoptosis of cultured mouse hepatocytes. Hepatology. 2004;40(5):1170–9. https://doi.org/10.1002/hep.20437.
45. Persson HJ, Yu Z, Tirosh O, Eaton JW, Brunk UT. Prevention of oxidant-induced cell death by lysosomotropic iron chelators. Free Radic Biol Med. 2003;34(10):1295–305.
46. Uchiyama A, Kim JS, Kon K, Jaeschke H, Ikejima K, Watanabe S, et al. Translocation of iron from lysosomes into mitochondria is a key event during oxidative stress-induced hepatocellular injury. Hepatology. 2008;48(5):1644–54. https://doi.org/10.1002/hep.22498.
47. Kangwansupamonkon W, Lauruengtana V, Surassmo S, Ruktanonchai U. Antibacterial effect of apatite-coated titanium dioxide for textiles applications. Nanomedicine. 2009;5(2):240–9. https://doi.org/10.1016/j.nano.2008.09.004.
48. Ray PC, Yu H, Fu PP. Toxicity and environmental risks of nanomaterials: challenges and future needs. J Environ Sci Health C Environ Carcinog Ecotoxicol Rev. 2009;27(1):1–35. https://doi.org/10.1080/10590500802708267.
49. Dudefoi W, Moniz K, Allen-Vercoe E, Ropers MH, Walker VK. Impact of food grade and nano-TiO_2 particles on a human intestinal community. Food Chem Toxicol. 2017;106(Pt A):242–9. https://10.1016/j.fct.2017.05.050.
50. Jo MR, Yu J, Kim HJ, Song JH, Kim KM, Oh JM, et al. Titanium dioxide nanoparticle-biomolecule interactions influence oral absorption. Nanomaterials (Basel). 2016;6(12):225. https://doi.org/10.3390/nano6120225.
51. Saber AT, Jacobsen NR, Mortensen A, Szarek J, Jackson P, Madsen AM, et al. Nanotitanium dioxide toxicity in mouse lung is reduced in sanding dust from paint. Part Fibre Toxicol. 2012;9:4. https://doi.org/10.1186/1743-8977-9-4.
52. Mura GM, Ganadu ML, Lubinu G, Maida V. Photodegradation of organic waste coupling hydrogenase and titanium dioxide. Ann N Y Acad Sci. 1999;879:267–75. https://doi.org/10.1111/j.1749-6632.1999.tb10430.x.
53. Foster HA, Ditta IB, Varghese S, Steele A. Photocatalytic disinfection using titanium dioxide: spectrum and mechanism of antimicrobial activity. Appl Microbiol Biotechnol. 2011;90(6):1847–68. https://doi.org/10.1007/s00253-011-3213-7.
54. Baines CP, Kaiser RA, Purcell NH, Blair NS, Osinska H, Hambleton MA, et al. Loss of cyclophilin D reveals a critical role for mitochondrial permeability transition in cell death. Nature. 2005;434(7033):658–62. https://doi.org/10.1038/nature03434.

55. Braydich-Stolle LK, Schaeublin NM, Murdock RC, Jiang J, Biswas P, Schlager JJ, et al. Crystal structure mediates mode of cell death in TiO_2 nanotoxicity. J Nanopart Res. 2009;11:1361–74. https://doi.org/10.1007/s11051-008-9523-8.
56. Mercer RR, Scabilloni JF, Hubbs AF, Battelli LA, McKinney W, Friend S, et al. Distribution and fibrotic response following inhalation exposure to multi-walled carbon nanotubes. Part Fibre Toxicol. 2013;10:33. https://doi.org/10.1186/1743-8977-10-33.
57. Mohamed HR. Estimation of TiOâ nanoparticle-induced genotoxicity persistence and possible chronic gastritis-induction in mice. Food Chem Toxicol. 2015;83:76–83. https://doi.org/10.1016/j.fct.2015.05.018.
58. Geng R, Ren Y, Rao R, Tan X, Zhou H, Yang X, et al. Titanium dioxide nanoparticles induced HeLa cell necrosis under UVA radiation through the ROS-mPTP pathway. Nanomaterials (Basal). 2020;10(10):2029. https://doi.org/10.3390/nano10102029.
59. Shi H, Magaya R, Castranova V, Zhao J. Titanium dioxide nanoparticles: e review of current toxicological data. Part Fibre Toxicol. 2013;10:15. https://doi.org/10.1186/1743-8977-10-15.
60. Häcker G. The morphology of apoptosis. Cell Tissue Res. 2000;301(1):5–17. https://doi.org/10.1007/s004410000193.
61. Li J, Yuan J. Caspases in apoptosis and beyond. Oncogene. 2008;27(48):6194–206. https://doi.org/10.1038/onc.2008.297.
62. Saraste A, Pulkki K. Morphologic and biochemical hallmarks of apoptosis. Cardiovasc Res. 2000;45(3):528–37. https://doi.org/10.1016/s0008-6363(99)00384-3.
63. Tucci P, Porta G, Agostini M, Dinsdale D, Iavicoli I, Cain K, et al. Metabolic effects of TiO2 nanoparticles, a common component of sunscreens and cosmetics, on human keratinocytes. Cell Death Dis. 2013;4(3):e549. https://doi.org/10.1038/cddis.2013.76.
64. de Duve C. Lysosomes revisited. Eur J Biochem. 1983;137(3):391–7. https://doi.org/10.1111/j.1432-1033.1983.tb07841.x.
65. Iversen TG, Skotland T, Sandvig K. Endocytosis and intracellular transport of nanoparticles: Present knowledge and need for future studies. Nanotoday. 2011;6(2):176–85. https://doi.org/10.1016/j.nantod.2011.02.003.
66. Kim JA, Åberg C, Salvati A, Dawson KA. Role of cell cycle on the cellular uptake and dilution of nanoparticles in a cell population. Nat Nanotechnol. 2011;7(1):62–8. https://doi.org/10.1038/nnano.2011.191.
67. Salvati A, Åberg C, dos Santos T, Varela J, Pinto P, Lynch I, et al. Experimental and theoretical comparison of intracellular import of polymeric nanoparticles and small molecules: toward models of uptake kinetics. Nanomedicine. 2011;7(6):818–26. https://doi.org/10.1016/j.nano.2011.03.005.
68. Xu Y, Wang J, Song X, Wei R, He F, Peng G, et al. Protective mechanisms of CA074-me (other than cathepsin-B inhibition) against programmed necrosis induced by global cerebral ischemia/reperfusion injury in rats. Brain Res Bull. 2016;120:97–105. https://doi.org/10.1016/j.brainresbull.2015.11.007.

69. Terman A, Kurz T, Gustafsson B, Brunk UT. Lysosomal labilization. IUBMB Life. 2006;58(9):531–9. https://doi.org/10.1080/15216540600904885.
70. Boya P, Kroemer G. Lysosomal membrane permeabilization in cell death. Oncogene. 2008;27(50):6434–51. https://doi.org/10.1038/onc.2008.310.
71. Kirkegaard T, Jäättelä M. Lysosomal involvement in cell death and cancer. Biochim Biophys Acta. 2009;1793(4):746–54. https://doi.org/10.1016/j.bbamcr.2008.09.008.
72. Stoka V, Turk V, Turk B. Lysosomal cysteine cathepsins: signaling pathways in apoptosis. Biol Chem. 2007;388(6):555–60. https://doi.org/10.1515/BC.2007.064.
73. Taurozzi JS, Hackley VA, Wiesner MR. Preparation of nanoscale TiO2 dispersion in biological test media for toxicological assessment. NIST Special Publication 1200-4 2012 http://dx.doi.org/10.6028/NIST.DP. 1200–4.
74. Akhtar MJ, Ahamed M, Alhadlaq H. Gadolinium oxide nanoparticles induce toxicity in human endothelial HUVECs via lipid peroxidation, mitochondrial dysfunction and autophagy modulation. Nanomaterials (Basel). 2020;10(9):1675. https://doi.org/10.3390/nano10091675.
75. Fotakis G, Timbrell JA. In vitro cytotoxicity assays: comparison of LDH, neutral red, MTT and protein assay in hepatoma cell lines following exposure to cadmium chloride. Toxicol Lett. 2006;160(2):171–7. https://doi.org/10.1016/j.toxlet.2005.07.001.
76. Gong J, Traganos F, Darzynkiewicz Z. A selective procedure for DNA extraction from apoptotic cells applicable for gel electrophoresis and flow cytometry. Anal Biochem. 1994;218(2):314–9. https://doi.org/10.1006/abio.1994.1184.
77. Nicoletti I, Migliorati G, Pagliacci MC, Grignani F, Riccardi C. A rapid and simple method for measuring thymocyte apoptosis by propidium iodide staining and flow cytometry. J Immunol Methods. 1991;139(2):271–9. https://doi.org/10.1016/0022-1759(91)90198-o.
78. Umansky SR, Korol' BA, Nelipovich PA. In vivo DNA degradation in the thymocytes of gamma-irradiated or hydrocortisone-treated rats. Biochim Biophys Acta. 1981;655(1):9–17. https://doi.org/10.1016/0005-2787(81)90060-5.
79. Han J, Burgess K. Fluorescent indicators for intracellular pH. Chem Rev. 2010;110(5):2709–28. https://doi.org/10.1021/cr900249z.
80. Sun XY, Gan QZ, Ouyang JM. Size-dependent cellular uptake mechanism and cytotoxicity toward calcium oxalate on Vero cells. Sci Rep. 2017;7:41949. https://doi.org/10.1038/srep41949.
81. Kirkland RA, Saavedra GM, Franklin JL. Rapid activation of antioxidant defenses by nerve growth factor suppresses reactive oxygen species during neuronal apoptosis: evidence for a role in cytochrome c redistribution. J Neurosci. 2007;27(42):11315–26. .

Figures

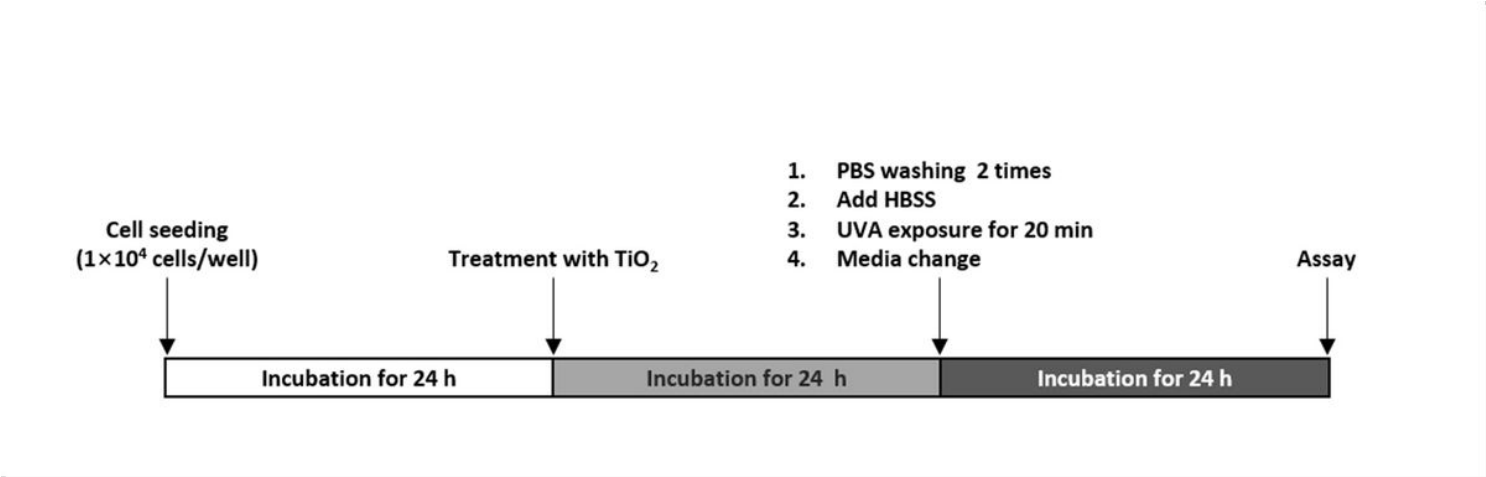

Figure 1

Outline of the experimental procedure

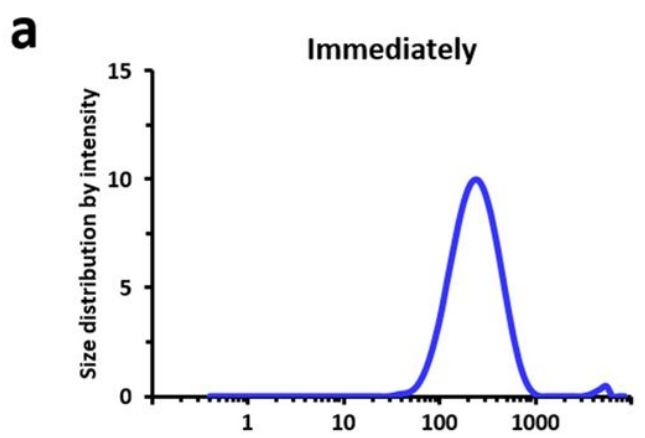

	Value
z-average (d, nm)	209.7±2.9
Polydispersity index	0.246

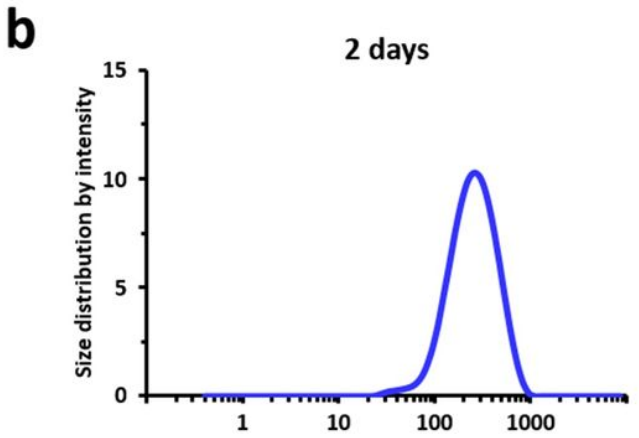

	Value
z-average (d, nm)	215.3±1.4
Polydispersity index	0.234

Figure 2

Characterization of TiO2 NPs in medium dispersion TiO2 NPs were dispersed at 1 mg/mL in DMEM. Size was measured by DLS immediately (a) and 2 days (b) after dispersion.

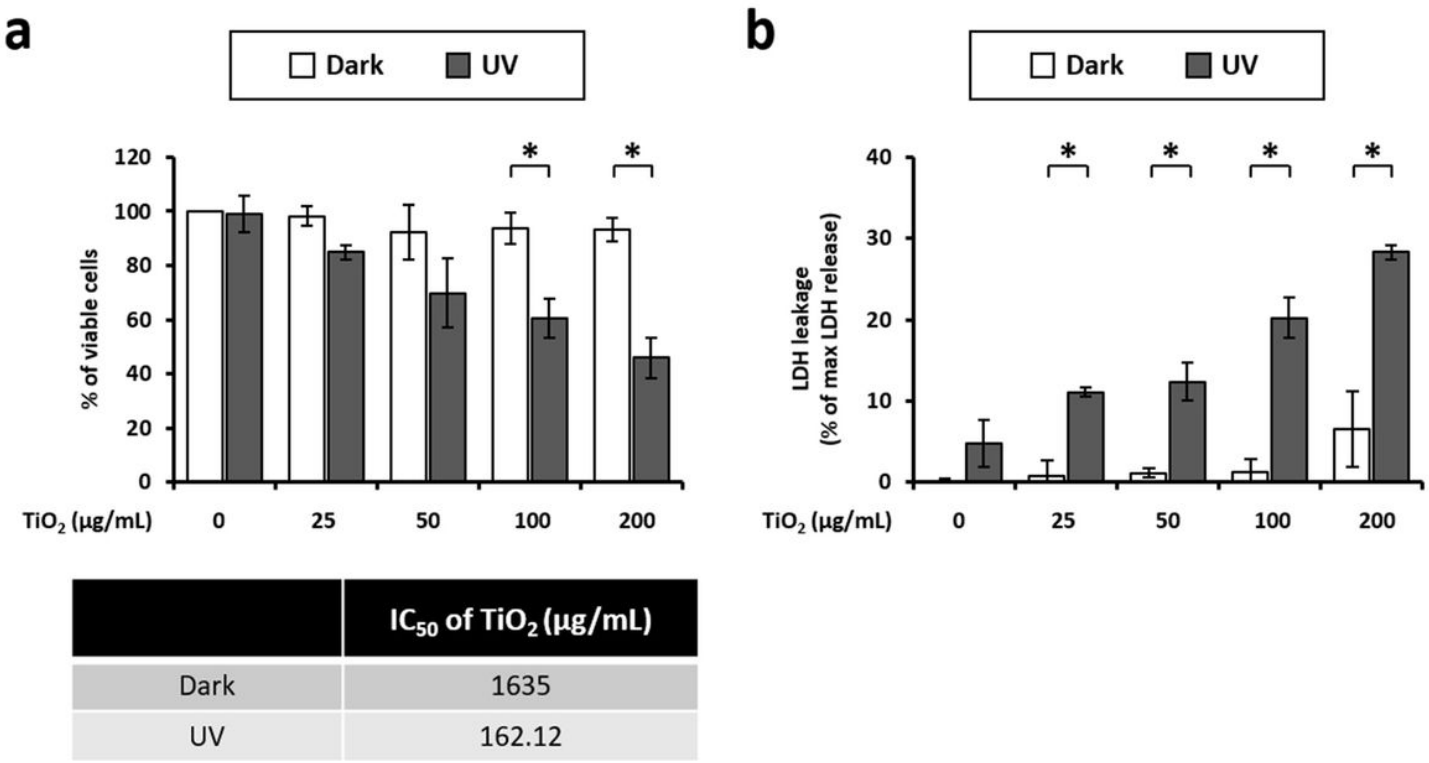

	IC_{50} of TiO_2 (µg/mL)
Dark	1635
UV	162.12

Figure 3

Effects of UVA exposure on HaCaT cells treated with TiO2 NPs (a) Cellular viability was evaluated using the CellTiter-Glo® Luminescent cell viability assay. (b) Lactate dehydrogenase (LDH) released by the cells was detected. Data are presented as mean ± SEM (n = 3). * P < 0.05, compared with dark conditions.

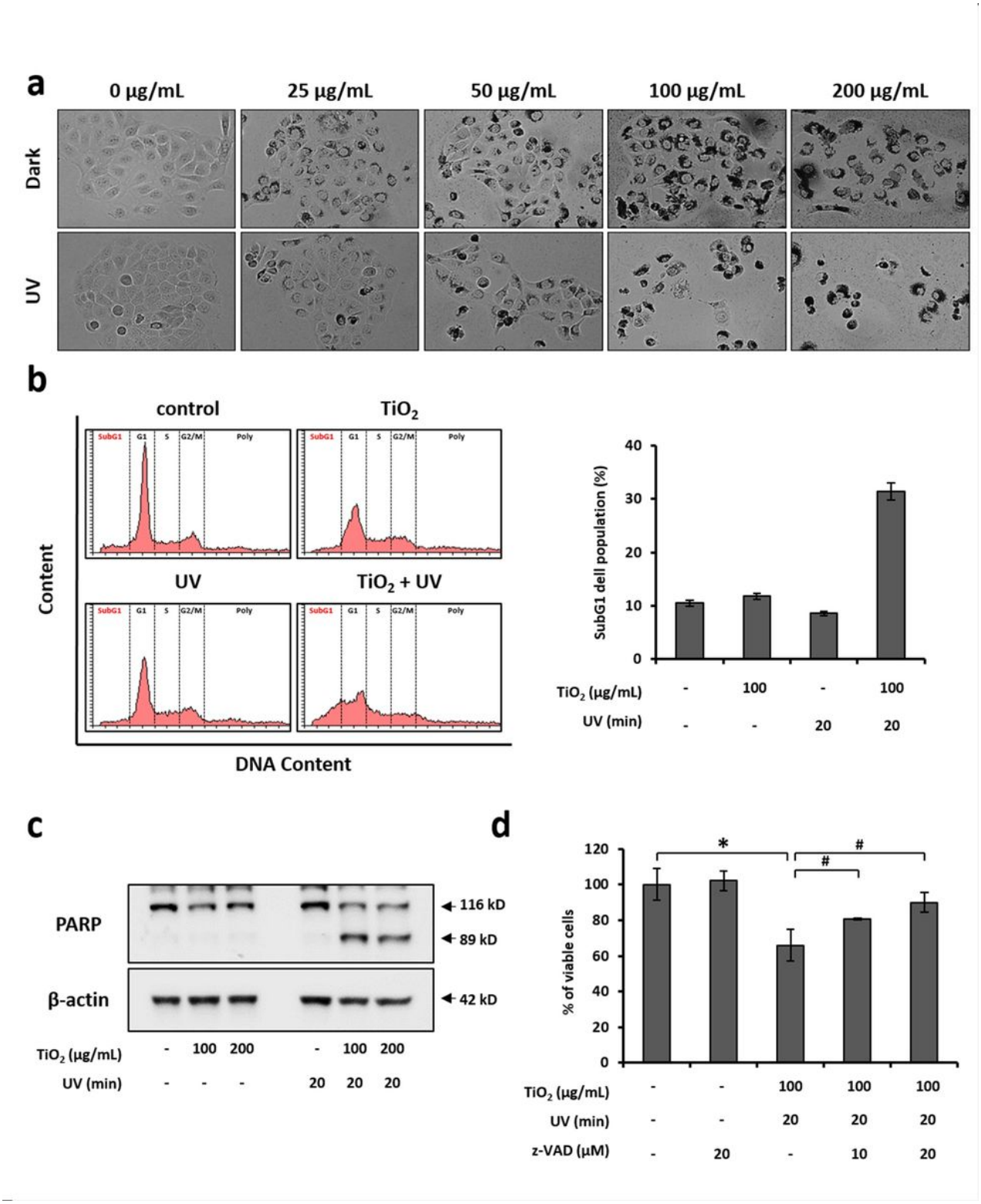

Figure 4

Apoptosis induction by the combination of TiO2 NPs and UVA (a) Treated cells were observed by bright-field microscopy. Bars, 20 μm. (b) HaCaT cells were treated with a combination of TiO2 NPs and UVA. The DNA content was measured by flow cytometry after PI staining. (c) Lysates were extracted from cells treated with TiO2 NPs and/or UVA. Western blotting of PARP was executed. β-Actin was the loading control. (d) The cells were treated with TiO2 NPs for 24 h and subsequently irradiated with UVA for 20

min. HBSS was replaced with the complete medium containing z-VAD-fmk, and the cells were incubated for 24 h. Cellular viability was determined using the CellTiter-Glo® Luminescent cell viability assay. Data are presented as mean ± SEM (n = 3). * P < 0.05, compared with the control; # P < 0.05, compared with the combination of TiO2 NPs and UVA.

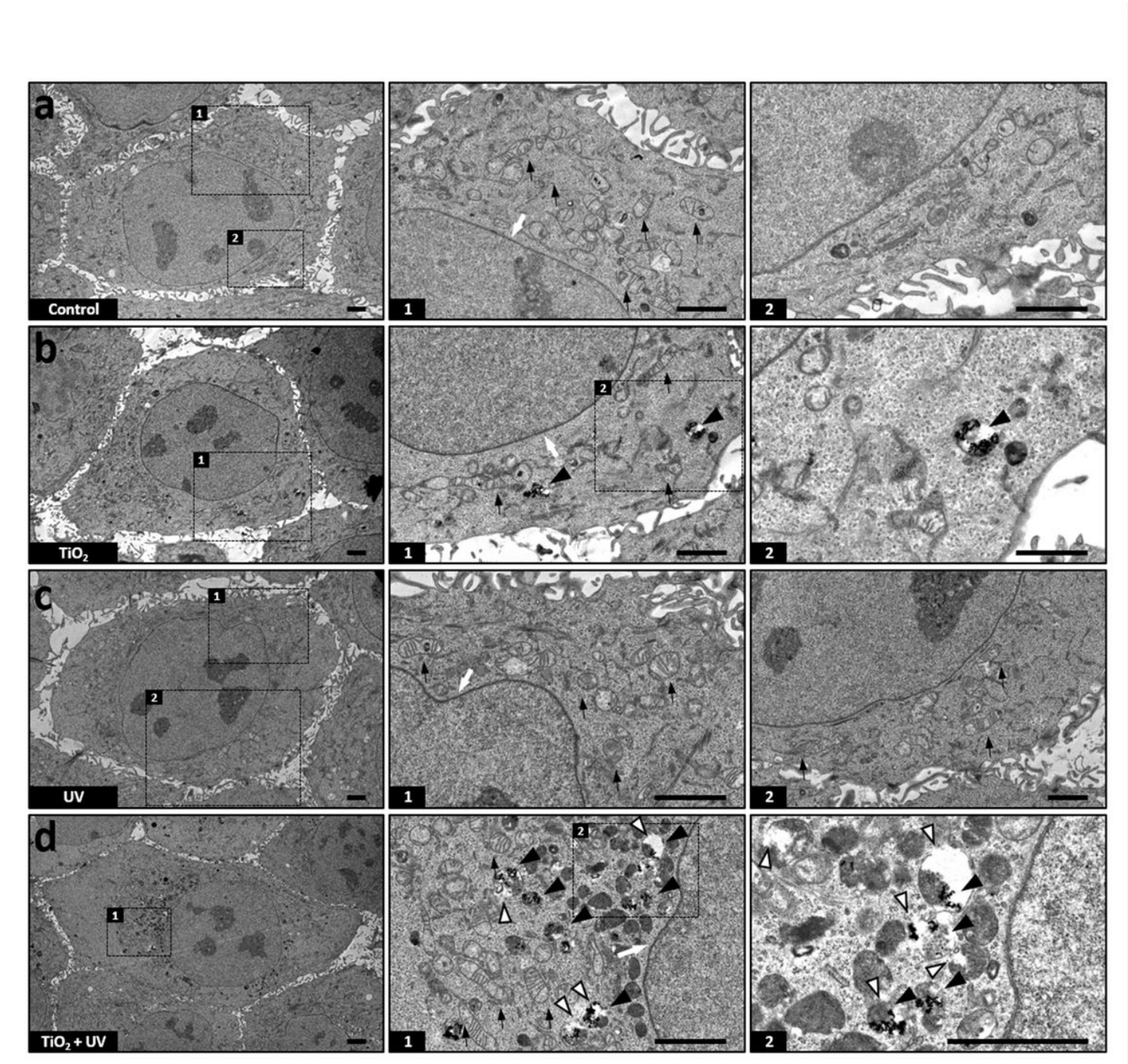

Figure 5

Transmission electron microscopy of HaCaT cells treated with TiO2 NPs and UVA (a) Untreated cells. (b) Cells treated with TiO2 NPs alone. (c) Cells irradiated with UVA for 20 min. (d) Cells co-treated with TiO2 NPs and UVA. Bars, 2 μm. Black arrowhead, phagosome-like structures; black arrow, mitochondria; white arrow, nuclei; white arrowhead, ruptured lysosome.

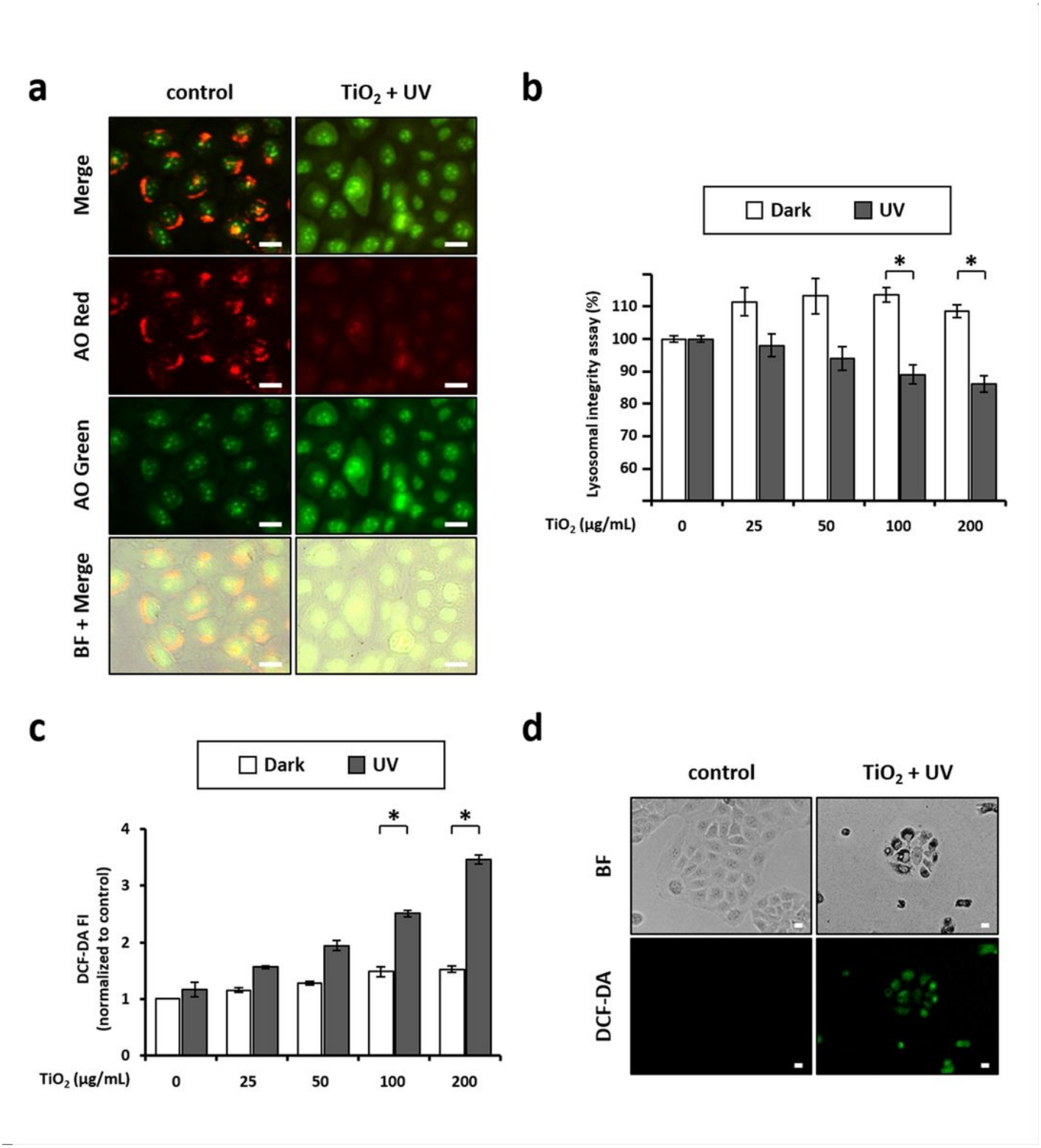

Figure 6

LMP induction and ROS generation by the combination of TiO2 NPs and UVA. (a) Treated cells were stained with AO, and then observed by fluorescence microscopy. Bars, 10 μm. (b) After AO staining, the cells were treated with TiO2 NPs and UVA for 8 h. The cells were subjected to microplate reading. Data are presented as mean ± SD (n = 8). * P < 0.05, compared with dark conditions. (c, d) The treated cells were stained with CM-H2DCF-DA. The cells were subjected to microplate reading. (c) Data are presented

as mean ± SD (n = 6). * P < 0.05, compared with dark conditions. (d) Cells were observed by fluorescence microscopy. Bars, 20 μm.

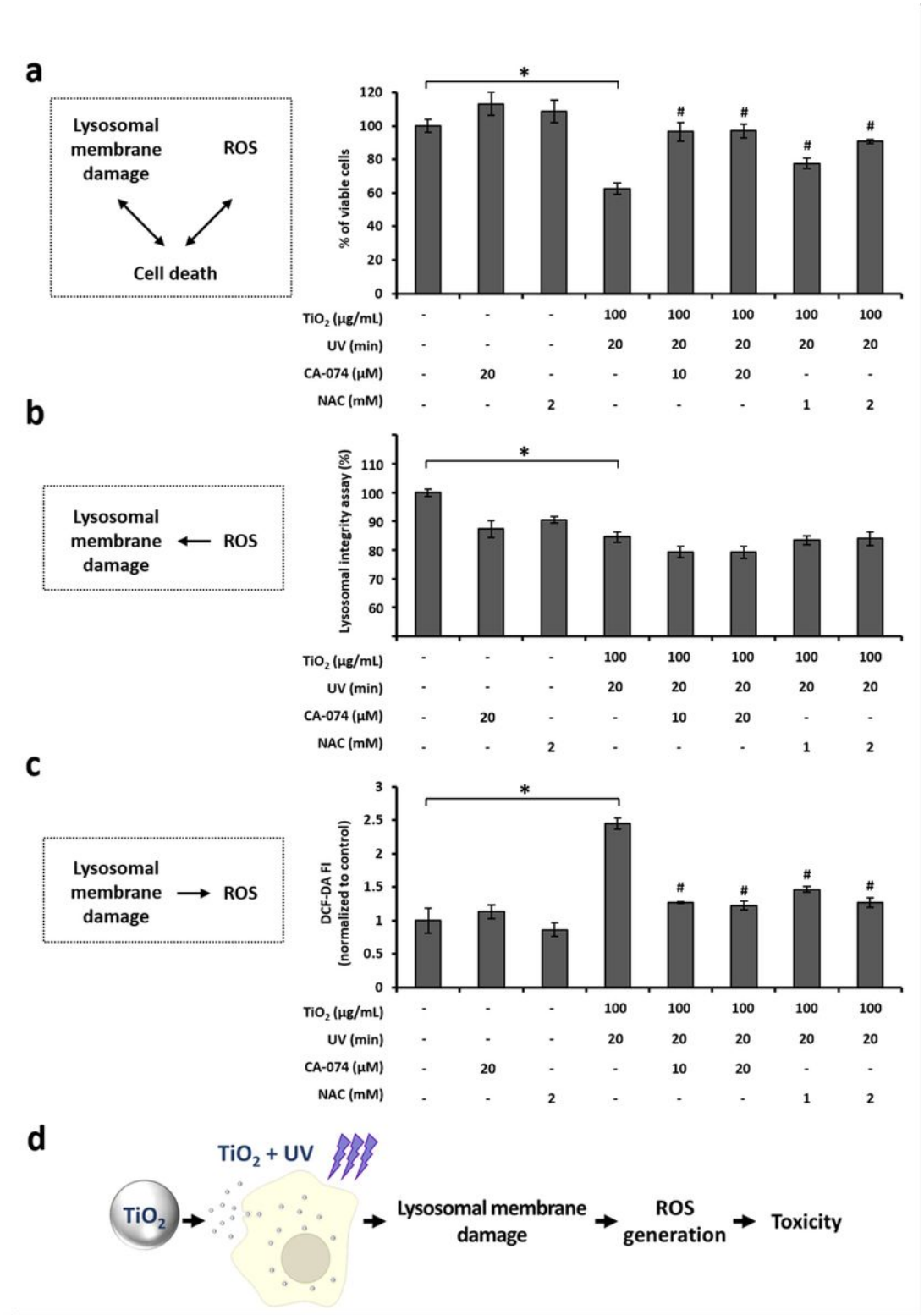

Figure 7

Interaction between cell death, LMP, and ROS in HaCaT cells treated with TiO2 NPs and UVA (a) The cells were treated with TiO2 NPs for 24 h and subsequently irradiated with UVA for 20 min. HBSS was replaced with the complete medium containing CA-074 or NAC, and the cells were incubated for 24 h. Cellular

viability was evaluated using the CellTiter-Glo® Luminescent cell viability assay. (b) After AO staining, the cells were treated with TiO2 NPs, UVA, and inhibitors for 8 h. The cells were then subjected to microplate reading. (c) The treated cells were stained with CM-H2DCF-DA. The cells were subjected to microplate reading. Data are presented as mean ± SD (n = 8). * $P < 0.05$, compared with untreated cells; # $P < 0.05$, compared with the combination of TiO2 NPs and UVA. (d) Hypothetical model for the underlying mechanisms of TiO2 NP and UVA-induced apoptosis.